applied sciences

MDPI

Article

An Efficient Approach for Fast and Accurate Voltage Stability Margin Computation in Large Power Grids

Heng-Yi Su

Department of Electrical Engineering, Feng Chia University (FCU), No. 100, Wenhwa Road, Seatwen, Taichung 40724, Taiwan; hengyisu@fcu.edu.tw; Tel.: +886-4-2451-7250 (ext. 3822)

Academic Editor: Josep M. Guerrero
Received: 14 September 2016; Accepted: 1 November 2016; Published: 3 November 2016

Abstract: This paper proposes an efficient approach for the computation of voltage stability margin (VSM) in a large-scale power grid. The objective is to accurately and rapidly determine the load power margin which corresponds to voltage collapse phenomena. The proposed approach is based on the impedance match-based technique and the model-based technique. It combines the Thevenin equivalent (TE) network method with cubic spline extrapolation technique and the continuation technique to achieve fast and accurate VSM computation for a bulk power grid. Moreover, the generator Q limits are taken into account for practical applications. Extensive case studies carried out on Institute of Electrical and Electronics Engineers (IEEE) benchmark systems and the Taiwan Power Company (Taipower, Taipei, Taiwan) system are used to demonstrate the effectiveness of the proposed approach.

Keywords: load power margin; voltage stability; voltage collapse point; voltage stability margin

1. Introduction

Voltage stability is a major concern and is the main factor that limits power transfers in today's grid operations. For this reason, significant research efforts have been devoted to understanding the voltage instability phenomenon and proposing corresponding countermeasures [1–3]. Voltage stability is an essential dynamic phenomenon. If analysis targets system load margin, critical bus identification, or reactive power compensation, then the use of static model is adequate. A large portion of studies have focused on the steady-state aspects of voltage stability. While static analysis is simple, it still provides some practical advantages over dynamic analysis, providing results with acceptable accuracy and little computational effort [4,5].

In several recent large-scale blackout events, such as in Scandinavia (2003), the northeastern United States (2003), southern Sweden (2003), eastern Denmark (2003), Italy (2003), Athens (2004), and Brazil (2009), voltage collapse has played a major role [6–8]. In view of this, it is essential for system operators to identify whether a current operating state is prone to voltage collapse or not. In order to measure system long-term voltage stability, the concept of voltage stability margin (VSM) has been proposed to demonstrate the closeness of current operating point to voltage collapse point [9,10]. A review of literature reveals that various VSM evaluation approaches are based on different kinds of techniques, such as sensitivity techniques [11,12], singular value decomposition techniques [13,14], machine learning techniques [15,16], impedance-based techniques [17–20], continuation techniques [21–24], and line voltage stability indices [25,26]. It is noteworthy that different voltage stability indices may give different results, i.e., they may not show the true distance to voltage collapse. An extensive comparison study on voltage stability indices can be found in the works [27,28].

In fact, voltage stability is related to saddle-node bifurcation, which corresponds to the maximum loading point [23]. When the generation-transmission system is unable to meet the continuous increase

in load demand, voltage instability and even voltage collapse situations are more likely to take place. In this regard, load power margin is often associated with VSM, as illustrated in Figure 1. Indeed, a number of methods proposed in works [21–24] utilize this kind of measure as a monitoring index of voltage stability.

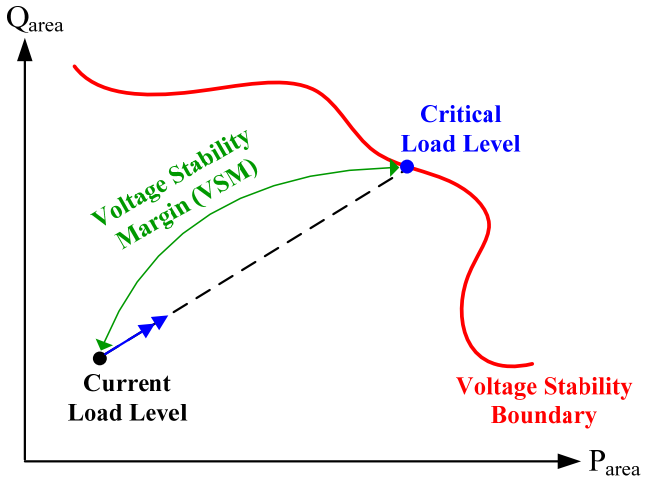

Figure 1. Illustration of voltage stability margin (VSM) in a load power parameter space.

To determine load power margin under a certain load level, *P-V* curves are widely utilized by power companies. Generally, such curves are generated by means of a series of power flow solutions for different load levels. However, successive computation using the traditional power flow approach may lead to a divergence problem near the voltage stability boundary. Thus, continuation power flow (CPFLOW)-based methods have been used to cope with the numerical difficulties caused by the singularity of the power-flow Jacobian matrix at and around the critical point [21–24]. Although CPFLOW based methods are able to track the exact voltage collapse point, these methods are time-consuming, especially for a large power grid model. Recently, some impedance match methods [17–20] have been proposed to determine the voltage collapse point. To the author's knowledge, most of these can quickly provide the results with acceptable accuracy.

The main contribution of this paper is the development of a new method for fast and accurate VSM computation in a large-scale power system. To this end, an efficient framework based on the impedance match-based technique and the model-based technique is proposed. In the proposed framework, the Thevenin equivalent (TE) network approach with cubic spline extrapolation technique and continuation technique are employed to determine the voltage collapse point. In addition, the developed approach is capable of dealing with the cases that cause generators to reach the Q limits. This paper is structured as follows: Section 2 presents the proposed algorithm for fast determination of voltage collapse point; this algorithm is applied to some Institute of Electrical and Electronics Engineers (IEEE) systems and the Taipower system, and the results are illustrated in Section 3. This paper finishes with some concluding remarks, drawn in Section 4.

2. Proposed Approach

In this research, an efficient method for fast as well as accurate VSM computation in large power grids is developed. This method combines both impedance match-based technique and model based technique. In addition, some practical operating conditions such as generator Q limit are taken into account for practical applications. The proposed framework is illustrated in Figure 2.

The following subsections present the detailed principles and methods used in the proposed framework.

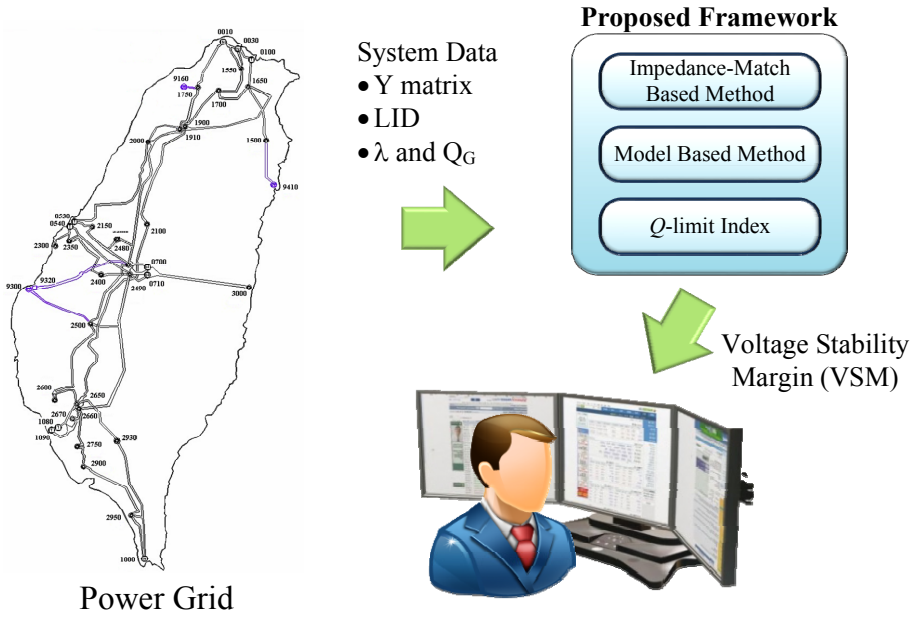

Figure 2. Proposed framework for determination of VSM. LID: the load increase direction; λ: the load increase parameter; Q_G: generator Q limits.

2.1. Multi-Node Thevenin Equivalent Circuit Model

A general multi-node network power system model is shown in Figure 3, where n_G generators and n_L loads are outside the transmission network. Such complex network can be converted into a multi-note TE network model. Let us begin with the relationship between the injected node currents and the node voltages given by

$$\mathbf{I} = Y_{bus}\mathbf{V} \tag{1}$$

where $\mathbf{I}$ is the vector of injected node currents; $\mathbf{V}$ is the vector of node voltages; Y_{bus} is the bus admittance matrix.

Due to three types of buses in the system, Equation (1) can be expressed as

$$\begin{bmatrix} \mathbf{I}_G \\ -\mathbf{I}_L \\ \mathbf{I}_T \end{bmatrix} = \begin{bmatrix} Y_{GG} & Y_{GL} & Y_{GT} \\ Y_{LG} & Y_{LL} & Y_{LT} \\ Y_{TG} & Y_{TL} & Y_{TT} \end{bmatrix} \begin{bmatrix} \mathbf{V}_G \\ \mathbf{V}_L \\ \mathbf{V}_T \end{bmatrix} \tag{2}$$

in which the subscripts G, L, and T are utilized to denote generator bus, load bus, and tie bus, respectively. From Equation (2), $\mathbf{V}_L$ can be expressed as

$$\mathbf{V}_L = K\mathbf{V}_G - Z\mathbf{I}_L \tag{3}$$

where

$$Z = \left(Y_{LL} - Y_{LT}Y_{TT}^{-1}Y_{TL}\right)^{-1} \tag{4}$$

$$K = -Z\left(Y_{LG} - Y_{LT}Y_{TT}^{-1}Y_{TG}\right) \tag{5}$$

In Equation (4), Z denotes the impedance matrix, and can be computed from Y_{bus}.

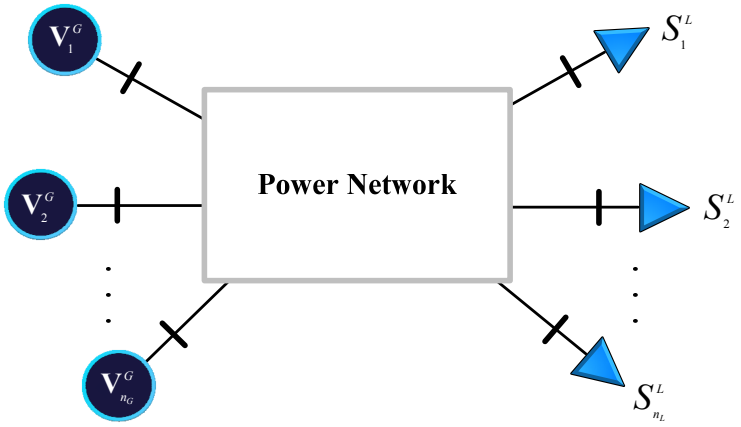

Figure 3. Multi-node network power system model. $\mathbf{V}^{\mathrm{G}}$, generator bus voltage; S^{L}, complex load power; n_{G}, number of generators; n_{L}, number of loads.

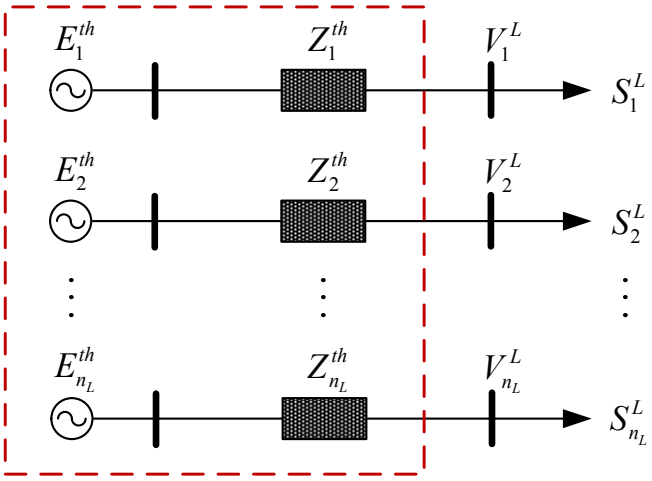

Figure 4. Multi-node Thevenin equivalent network model. $\mathbf{E}^{\mathrm{th}}$, Thevenin equivalent voltage; Z^{th}, Thevenin equivalent impedance; $\mathbf{V}^{\mathrm{L}}$, load bus voltage; red dashed box, Thevenin equivalent; arrows, load demand.

Figure 4 illustrates a multi-node TE network model for the representation of Equation (3). For any load bus $i \in \{1, \cdots, n_{\mathrm{L}}\}$, we have

$$\mathbf{V}_i^{\mathrm{L}} = \mathbf{E}_i^{\mathrm{th}} - Z_i^{\mathrm{th}} \mathbf{I}_i^{\mathrm{L}} \tag{6}$$

where

$$\mathbf{E}_i^{\mathrm{th}} = [K\mathbf{V}_{\mathrm{G}}]_i - \sum_{j=1, j\neq i}^{n} Z_{ij} \mathbf{I}_j^{\mathrm{L}} \tag{7}$$

$$Z_i^{\mathrm{th}} = Z_{ii} \tag{8}$$

$\mathbf{E}_i^{\mathrm{th}}$ and Z_i^{th} correspond to TE voltage and TE impedance at load bus i, respectively. Z_{ij} is the i-j element of Z and Z_{ii} is the diagonal element of Z. In addition, the load impedance of the complex load power S_i^{L} is given by

$$Z_i^{\mathrm{L}} = \frac{\left|\mathbf{V}_i^{\mathrm{L}}\right|^2}{\left(S_i^{\mathrm{L}}\right)^*} \tag{9}$$

where $\left(S_i^{\mathrm{L}}\right)^*$ denotes the conjugate of S_i^{L}.

2.2. Cubic Spline Extrapolation Technique

In Figure 4, as voltage collapse occurs at bus i, the impedance-matching criterion holds; i.e., $\left|Z_i^{\mathrm{L}}\right| = \left|Z_i^{\mathrm{th}}\right|$. Thus, the estimated maximum loading point at which voltage collapses can be made by equating an approximate function, that extrapolates the trajectory of $\left|Z_i^{\mathrm{L}}\right|$, to $\left|Z_i^{\mathrm{th}}\right|$. A cubic spline function is selected as the approximate function in this study. The fundamental idea behind constructing a spline function is to divide the interval into a collection of subintervals and construct a different approximating low-order polynomial in each subinterval. In cubic splines, third-order polynomials are used in the subintervals between each pair of data points. Thus, the curves obtained from each subinterval are smooth.

For example, given m data points, there are $m-1$ subintervals, and the equation of the polynomial in the jth subinterval is expressed as

$$f_j(z) = a_j + b_j\left(z - z_j\right) + c_j\left(z - z_j\right)^2 + d_j\left(z - z_j\right)^3 \tag{10}$$

for each $j = 1, 2, \cdots, m-1$. Overall, there are $m-1$ equations. Since each third-order polynomial has four coefficients, a total of $4\left(m-1\right) = 4m-4$ unknowns have to be determined. All of the coefficients a_j, b_j, c_j, and d_j can be found by applying the method proposed in [29]. In this work, the variable x in Equation (10) is replaced with the calculated $\left|Z_i^{\mathrm{L}}\right|$, and m is set to three.

The cubic spline extrapolation function is constructed by the coordinates of the given data points $\left(\left|Z_i^{\mathrm{L}}\right|, \lambda\right)$, where λ denotes the load increase parameter. The function is then used for calculating the extrapolated value of $\left|Z_i^{\mathrm{L}}\right| = \left|Z_i^{\mathrm{th}}\right|$. Since m is set to three, the inputs to the function are three sets of data points $\left(\left|Z_i^{\mathrm{L}}\right|, \lambda\right)$ and the point of $\left|Z_i^{\mathrm{th}}\right|$. The output from the function is the estimated maximum load point λ^{es}.

2.3. Generator Q-Limit Index

Figure 5a depicts $\left|Z^{\mathrm{L}}\right|$ and $\left|Z^{\mathrm{th}}\right|$ as a function of load increase without violations of generator Q limits. The solid line shown in Figure 5a denotes the function curve for extrapolation with cubic splines. Observations from extensive simulations on power systems ranging from small to large power grids indicate that, using the approach above, the estimated λ^{es} (which is close to but a little less than the exact λ^{max}), can be acquired.

For those cases with generator Q limit violation during load increase, Z in Equation (5) must be updated based on the change of bus type status (PV bus to PQ bus) before the estimation of λ^{es}. An illustrative example of Q limit violation is depicted in Figure 5b, where the sharp jump in $\left|Z^{\mathrm{th}}\right|$ coincides with the generator reaching its capacity limits. In this study, a Q-limit index $Q_{\mathrm{G}i}^{\mathrm{ex}}$ proposed in [20] is used to measure the extreme Q for each generator based on the given load increase direction (LID). The process for identifying generator Q limit violation is summarized in Algorithm 1. According to [20], the approximation quadratic model of $\lambda - Q_{\mathrm{G}}$ curve can be described as $\lambda = \alpha_i Q_{\mathrm{G}i}^2 + \beta_i Q_{\mathrm{G}i} + \gamma_i$, where α_i, β_i, and γ_i can be obtained by utilizing three sets of λ and $Q_{\mathrm{G}i}$. Once the coefficients are determined, the extreme value of $Q_{\mathrm{G}i}$, denoted by $Q_{\mathrm{G}i}^{\mathrm{ex}}$, can be estimated. When $Q_{\mathrm{G}i}^{\mathrm{ex}} \le Q_{\mathrm{G}i}^{\mathrm{min}}$ or $Q_{\mathrm{G}i}^{\mathrm{ex}} \ge Q_{\mathrm{G}i}^{\mathrm{max}}$, generator Q limits occur at PV bus i, in which $Q_{\mathrm{G}i}^{\mathrm{min}}$ and $Q_{\mathrm{G}i}^{\mathrm{max}}$ are the lower and upper limits of the ith generator. Otherwise, there is no generator Q limit violation at PV bus i. After the execution of Algorithm 1 for $\{Q_{\mathrm{G}i}\}_{i=1}^{n_{\mathrm{G}}}$, a list of Q limit violations at PV buses is obtained.

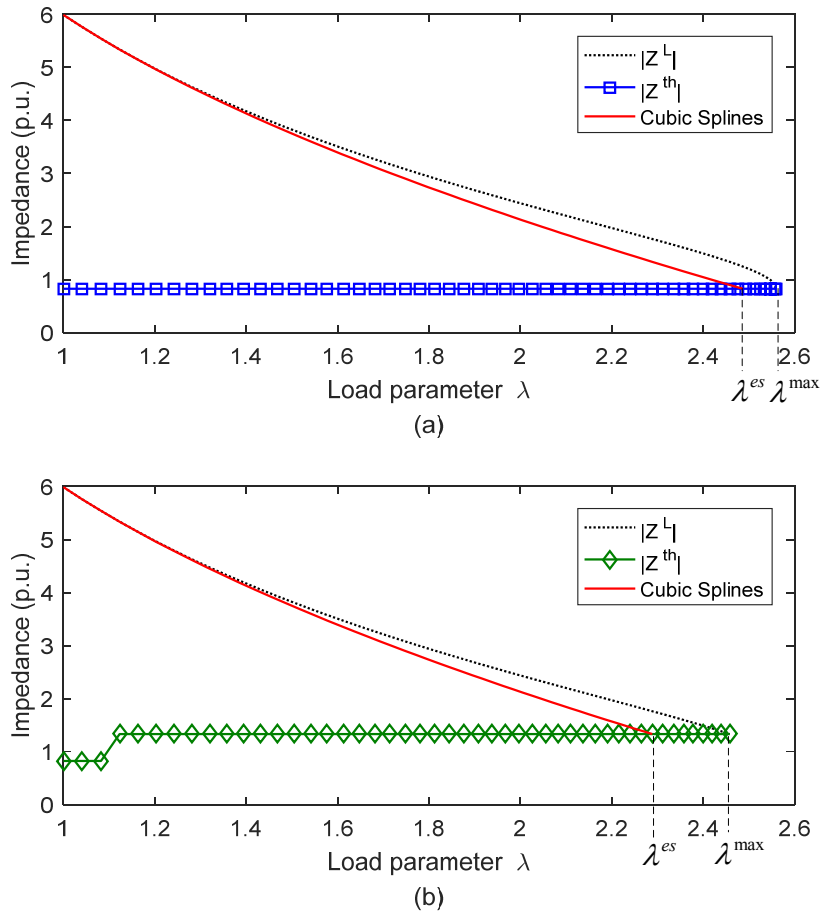

Figure 5. Illustration of the cubic spline extrapolation technique for estimation of $\lambda^{\max}$. (**a**) Case without Q limit violations; (**b**) Case with a Q limit violation.

Algorithm 1. Identify generator Q limit violations.

Input: $D = \{Q_{Gi}(k), \lambda(k)\}_{k=1}^{3}$ for $i \in \{PV\}$ and LID;
function QLIMIT(D)
Find α_i, β_i, γ_i by solving $\lambda = \alpha_i Q_{Gi}^2 + \beta_i Q_{Gi} + \gamma_i$;
$Q_{Gi}^{ex} \leftarrow -\frac{\beta_i}{2\alpha_i}$;
if $Q_{Gi}^{ex} \leq Q_{Gi}^{min}$ or $Q_{Gi}^{ex} \geq Q_{Gi}^{max}$ **then**
Bus type change for bus i (PV bus to PQ bus);
end if
return List of Q limit violations
end function

2.4. Continuation Technique

Although the proposed approach for determination of $\lambda^{\max}$ is independent of the model-based tool selected, the continuation method proposed in [22] was applied in this work. One feature of this approach is that it remains well-conditioned at all possible loading conditions in power flow calculation.

Consider the following steady-state power system models

$$F(\mathbf{y}, \lambda) = \mathbf{0} \tag{11}$$

where **y** denotes the vector of bus voltage phasors; λ represents the load increase parameter.

The continuation approach is based on a locally parameterized continuation technique. Indeed, it is an iterative calculation process which starts from a known operating point and is solved as $F(\mathbf{y}, \lambda) = \mathbf{0}$ as λ changes. In addition, the predictor-corrector scheme is utilized to find each solution of the manifold.

A widely accepted voltage stability measure can be expressed by the load power margin, i.e., $\lambda^{\max} - \lambda^0$, where λ^0 represents the base case loading point. Hence, VSM defined by the percentage of $\lambda^{\max} - \lambda^0$ is

$$VSM = \frac{\lambda^{\max} - \lambda^0}{\lambda^0} \times 100\% \tag{12}$$

In summary, the proposed method aims to quickly determine the proximity to voltage collapse. It can cope with the cases that cause generators reaching their Q limits. The computation process to determine VSM is summarized in Algorithm 2. The input of this algorithm is Y_{bus} and three sets of $|Z^{\text{L}}|$, λ, and Q_{G}, and the output is VSM.

The main steps in Algorithm 2 for finding VSM are described as follows:

(1) Compute $Q_{\text{G}i}^{\text{ex}}$ for $i \in \{PV\}$ to create a list of Q limit violations L_{PV}^{PQ};
(2) Employ a multi-node Thevenin equivalent network to model a power system. Next, calculate $\left|Z_j^{\text{th}}\right|$ and $\left|Z_j^{\text{L}}\right|$ for $j \in \{PQ\}$ based on L_{PV}^{PQ};
(3) Utilize cubic spline extrapolation technique to estimate λ^{es} based on $\left|Z_j^{\text{th}}\right|$ and $\left|Z_j^{\text{L}}\right|$;
(4) Execute a continuation program to determine the exact $\lambda^{\max}$ through the information of λ^{es};
(5) Compute VSM via Equation (12).

Algorithm 2. Determine VSM via the proposed method.

Input: Y_{bus}, three sets of Q_{G}, λ, and $\left|Z_j^{\text{L}}\right|$;
$D \leftarrow \{Q_{\text{G}i}(k), \lambda(k)\}_{k=1}^{3}$;
for $i \in \{PV\}$ **do**
$L_{PV}^{PQ} \leftarrow Q\text{LIMIT}(D)$;
end for
Compute Z by Equation (4) based on L_{PV}^{PQ};
Compute $\left|Z_j^{\text{th}}\right|$ for $j \in \{PQ\}$ by Equation (8);
Estimate λ^{es} via cubic spline extrapolation technique;
Determine $\lambda^{\max}$ based on λ^{es} via a continuation program;
Compute VSM by Equation (12);
return VSM

3. Simulation Results

The proposed approach is applied to some IEEE test systems and a real power system. The scenarios, that are evaluated, are summarized in Figure 6. The experiments are implemented in MATLAB® (R2009b, Torrance, CA, USA, 2009), and run on an Intel® Core™2 Duo 2.66 GHz computer (ASUS, Taipei, Taiwan) with 4 GB of RAM (random access memory). In addition, CPU (central processing unit) time is an important metric for verifying the performance of the proposed approach. The CPU time was measured by using the MATLAB *cputime* function [30] in our program. The simulation results obtained were all compared with those found by the conventional CPFLOW approach. More details are illustrated and discussed in the cases below.

Scenario	IEEE 30-bus - Generator: 6 - Load : 24 - Branch : 41	IEEE 118-bus - Generator: 54 - Load : 64 - Branch : 186	Taipower - Generator: 271 - Load : 1538 - Branch : 3319
Load Level	Different load levels		
Load Pattern	Single load change Multiple load change		
N-1 Contingency	Branch outage contingnecy		

Figure 6. Summary of scenarios and events during the experiments. IEEE: Institute of Electrical and Electronics Engineers.

3.1. Effects of Different Load Increase Scenarios

In this research, the single load bus variation and multiple load bus variation are considered. Also, the load increase direction simulated in the experiments is based on the initial load level at each bus.

3.1.1. IEEE 30-Bus System

The first test system is concerned with the IEEE 30-bus system that consists of 6 generators, 24 loads, and 41 lines [31].

In the first phase of the simulation, single load change case is tested wherein the load at the specific bus is increased proportionally until the load flow equations fail to converge. In this simulation, the load at bus 30 is selected. Figure 7 shows the comparison with λ^{max} and CPU time with the proposed method and conventional CPFLOW method, where λ^{max} denotes the critical point at which voltage collapses. From the shown figure, one can see that both the proposed approach and conventional CPFLOW approach can achieve the actual value $\lambda^{max} = 1.8777$. The CPU time, however, is quite different from each method. Specifically, the proposed method takes 0.23 s in the execution, while the conventional CPFLOW method takes 0.86 s.

In the second phase of the simulation, a multiple load change case is considered. In this case, all the loads in the test system are simultaneously increased with a constant load power factor. The trajectories of searching λ^{max} using the two compared methods are given in Figure 8. It indicates that the proposed method quickly finds the accurate solution of $\lambda^{max} = 2.9493$ in 0.29 s. Meanwhile, for the conventional CPFLOW method, it still requires 1.15 s to reach the same point.

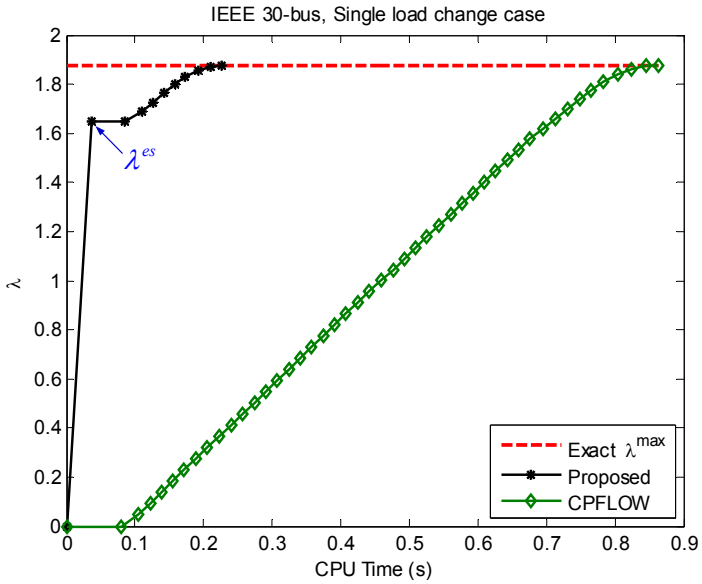

Figure 7. Comparison with λ^{max} and CPU (central processing unit) time between the proposed approach and conventional continuation power flow (CPFLOW) approach under single load change scenario on IEEE 30-bus system: proposed approach, λ^{max} = 1.8777, CPU = 0.23 s: conventional CPFLOW approach, λ^{max} = 1.8777, CPU = 0.86 s.

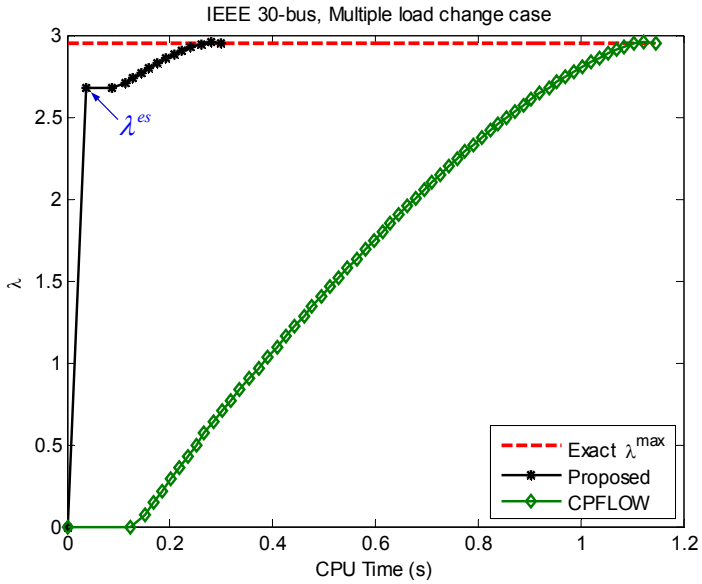

Figure 8. Comparison with λ^{max} and CPU time between the proposed approach and conventional CPFLOW approach under multiple load change scenario on an IEEE 30-bus system: proposed approach, λ^{max} = 2.9493, CPU = 0.29 s; conventional CPFLOW approach, λ^{max} = 2.9493, CPU = 1.15 s.

3.1.2. IEEE 118-Bus System

The IEEE 118-bus system is also used as a test model to illustrate the applicability of the proposed approach to large power grids. This test system composes of 54 generators, 64 loads, and 186 lines [31].

An illustrative example of the single load bus variation (load increase at bus 118) is shown in Figure 9. The CPU times are 1.95 s for the proposed method and 11.27 s for the conventional CPFLOW method. Figure 10 illustrates another test result for the multiple load bus variation (load increase at all buses). The CPU time from this case for the proposed method and CPFLOW method are 2.15 and

6.58 s, respectively. From the two cases presented, it is clearly observed that the proposed approach is faster and runs more efficiently, compared to the conventional CPFLOW approach.

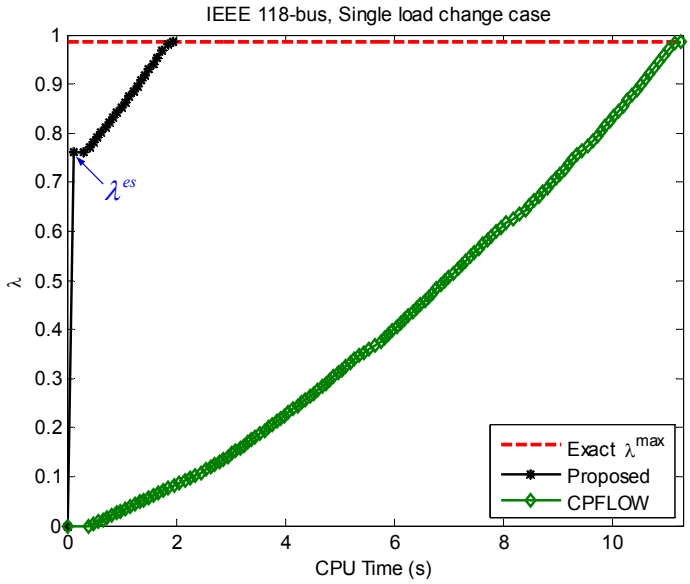

Figure 9. Comparison with $\lambda^{max}$and CPU time between the proposed approach and conventional CPFLOW approach under single load change scenario on IEEE 118-bus system: proposed approach, λ^{max} = 0.9868, CPU = 1.95 s; conventional CPFLOW approach, λ^{max} = 0.9868, CPU = 11.27 s.

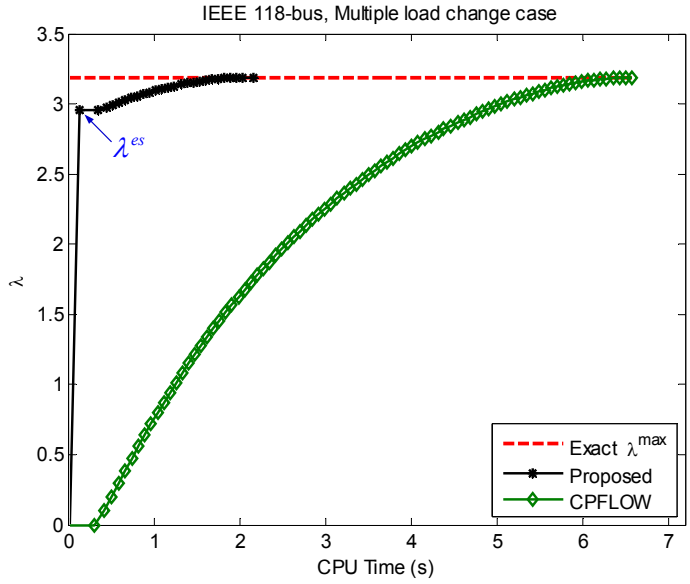

Figure 10. Comparison with λ^{max} and CPU time between the proposed approach and conventional CPFLOW approach under multiple load change scenario on IEEE 118-bus system: proposed approach, λ^{max} = 3.1871, CPU = 2.15 s: conventional CPFLOW approach, λ^{max} = 3.1871, CPU = 6.58 s.

3.2. Effects of Q Limits Violation

To investigate the impact of *Q* limit violations on VSM computation, we have studied many cases, including various load patterns, various load levels, and various *Q* limit violations. Among those investigated cases, some selected simulation scenarios are listed in Table 1.

Table 1. Scenarios for the test system.

Case	Load Pattern [1]	*Q* Limit [2]
1	Load_All	QG_All
2	Load_All	QG_Odd
3	Load_All	QG_Even
4	Load_Odd	QG_All
5	Load_Odd	QG_Odd
6	Load_Odd	QG_Even
7	Load_Even	QG_All
8	Load_Even	QG_Odd
9	Load_Even	QG_Even
10	Load_One	QG_All
11	Load_One	QG_Odd
12	Load_One	QG_Even

[1] Load Pattern: Load_All, Load_Odd, Load_Even and Load_One denote load increases at all load buses, at odd load buses, at even load buses, and at a load bus, respectively; [2] QG: generator *Q* limits. *Q* Limit: QG_All, QG_Odd, and QG_Even denote *Q* limits at all generator buses, at odd generator buses, and at even generator buses, respectively.

The simulation results for the IEEE 30-bus and IEEE 118-bus are presented in Tables 2 and 3, respectively. The output is organized in five columns: the first column depicts the test case which scenario is listed in Table 1. The simulation results of λ^{max} computed by the proposed approach and CPFLOW approach are given in column 2 and column 3. The last two columns depict the results of CPU time (s) computed by the proposed approach and CPFLOW approach. From Tables 2 and 3, it is once again shown that the proposed approach is able to provide an accurate solution with a shorter computation time.

Table 2. Performance comparison between the proposed approach and CPFLOW approach for IEEE 30-Bus system [1].

Case	λ^{max}		VSM (%)		CPU Time (s)	
	Proposed	CPFLOW	Proposed	CPFLOW	Proposed	CPFLOW
1	2.3328	2.3328	70.29	70.29	0.32	1.22
2	1.5552	1.5552	10.11	10.11	0.39	1.28
3	1.8229	1.8229	28.72	28.72	0.39	1.27
4	2.8577	2.8577	82.45	82.45	0.35	1.24
5	2.5215	2.5215	74.97	74.97	0.38	1.29
6	2.3167	2.3167	51.35	51.35	0.31	1.21
7	1.5116	1.5116	6.49	6.49	0.34	1.25
8	2.0565	2.0565	49.95	49.95	0.38	2.14
9	1.6337	1.6337	20.15	20.15	0.37	1.27
10	2.7236	2.7236	80.16	80.16	0.39	1.27
11	2.1221	2.1221	39.98	39.98	0.36	1.22
12	2.0174	2.0174	37.69	37.69	0.31	1.25

[1] VSM, voltage stability margin; CPFLOW, conventional continuation power flow.

Table 3. Performance comparison between the proposed approach and CPFLOW approach for IEEE 118-Bus system.

Case	λ^{max}		VSM (%)		CPU Time (s)	
	Proposed	CPFLOW	Proposed	CPFLOW	Proposed	CPFLOW
1	2.6405	2.6405	38.76	38.76	2.95	11.81
2	3.1871	3.1871	50.29	50.29	3.14	10.42
3	1.4769	1.4769	6.31	6.31	3.21	12.45
4	1.5283	1.5283	14.41	14.41	3.25	10.54
5	2.1263	2.1263	23.73	23.73	2.78	11.51

Table 3. *Cont.*

Case	λ^{max}		VSM (%)		CPU Time (s)	
	Proposed	CPFLOW	Proposed	CPFLOW	Proposed	CPFLOW
6	1.7207	1.7207	14.81	14.81	3.18	12.25
7	2.8146	2.8146	48.78	48.78	3.15	12.99
8	2.6706	2.6706	44.97	44.97	2.67	13.25
9	1.8404	1.8404	19.92	19.92	2.63	11.67
10	2.6282	2.6282	32.45	32.45	2.99	10.09
11	2.2282	2.2282	27.54	27.54	3.45	10.13
12	2.4259	2.4259	30.15	30.15	2.84	10.55

3.3. Taiwan Power (Taipower) System

The proposed algorithm has been tested on a real power system, the Taipower system, which is a narrow and long power grid covering a distance of 400 km from north to south. Usually it is divided into three areas: north, center, and south. Different areas are connected together via a number of 345 kV transmission lines, as shown in Figure 11. This sample system is composed of 1821 buses and 3319 lines.

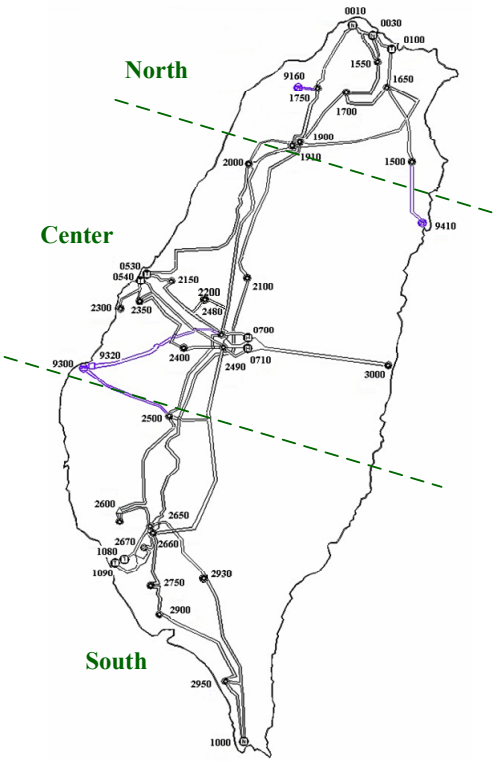

Area	Bus No.	Bus Name	Bus No.	Bus Name
North	0010	1st Nuclear	1700	Pan Chiao
	0030	2nd Nuclear	1750	Ting Hu
	0100	Hsieho	1900	Lung Tan (N)
	1500	Tung Shan	1910	Lumg Tan (S)
	1550	His Chin	9160	Kuo Kuang
	1650	Shen Mei		

Area	Bus No.	Bus Name	Bus No.	Bus Name
Center	0530	Chung Huo (N)	2350	Chuan Hsing
	0540	Chung Huo (S)	2400	Nan Tou
	0700	Ta Kuan 2	2480	Chung Liao (N)
	0710	Ming Tan	2490	Chung Liao (S)
	2000	O Mei	3000	Feng Lin
	2100	Tien Lun	9300	Mai Liao
	2200	Wu Feng	9320	Su Hua
	2150	Chung Kang	9410	Ho Ping
	2300	Chang Pina		

Area	Bus No.	Bus Name	Bus No.	Bus Name
South	1000	3rd Nuclear	2660	Lung Chi (S)
	1080	Hsin Ta (N)	2670	Lu Pei
	1090	Hsin Ta (S)	2750	Jen Wu
	2500	Chia Min	2900	Kao Kang
	2600	Nan Ko	2930	Mi Li
	2650	Lung Chi (N)	2950	Ta Peng

Figure 11. Simplified diagram of Taipower system.

In this work, many test cases on Taipower system have been studied. These include various system conditions and loading conditions. Moreover, generator Q limits are taken into account in each simulation. The comparisons with the selected cases listed in Table 1 are shown in Table 4. This table indicates that the proposed approach is capable of offering accurate λ^{max} as well as being time efficient.

Table 4. Performance comparison between the proposed approach and CPFLOW approach for Taipower system.

Case	λ^{max}		VSM (%)		CPU Time (s)	
	Proposed	**CPFLOW**	**Proposed**	**CPFLOW**	**Proposed**	**CPFLOW**
1	1.4223	1.4223	23.16	23.16	125.36	506.22
2	1.3839	1.3839	18.69	18.69	118.08	510.17
3	1.2641	1.2641	9.56	9.56	127.28	511.98
4	1.2022	1.2022	5.87	5.87	117.89	525.42
5	1.3817	1.3817	17.14	17.14	128.76	523.11
6	1.5732	1.5732	42.12	42.12	125.87	514.41
7	1.2587	1.2587	15.68	15.68	120.22	520.35
8	1.4059	1.4059	22.61	22.61	129.21	526.41
9	1.2831	1.2831	11.89	11.89	129.97	529.56
10	1.4164	1.4164	22.48	22.48	118.79	518.15
11	1.5185	1.5185	38.53	38.53	130.51	530.76
12	1.4611	1.4611	33.96	33.96	119.44	522.49

3.4. Statistical Evalution

Extensive case studies with respect to various test systems, various load patterns, various load levels, and various *Q*-limit violations have been conducted. The proposed approach can accurately and rapidly determine the point of voltage collapse for all tested cases. The statistical results are summarized in the following.

The average timing results under the selected 500 simulation runs for each test system are listed in Table 5, showing that the average CPU time of the proposed approach is about three to four times faster than that of the the conventional CPFLOW approach. This means that a fast computation of voltage collapse point can be achieved by using the proposed method.

Table 5. Comparison of average CPU time (s) under 500 simulation runs for the test system.

Test System	No. of Generators	No. of Loads	No. of Lines	Average CPU Time (s)	
				Proposed	**CPFLOW**
IEEE 30-bus	6	24	41	0.36	1.25
IEEE 118-bus	54	64	186	3.03	11.81
Taipower	271	1538	3319	121.27	502.08

3.5. N-1 Contingency Analysis

The effectiveness of the proposed approach to *N*-1 contingency situation, which is the normal system minus one component, was evaluated. In this work, the considered single contingency conditions are outages of lines and outages of generators.

The IEEE 30-bus system was selected as an example to illustrate the performance of the proposed method to branch outages. Table 6 summarizes the contingency ranking list for the IEEE 30-bus test system. In this table, column 2 denotes different branch outage scenarios and these contingencies are ranked by severity order in terms of λ^{max} given in column 3. A smaller value of λ^{max} results in a more severe branch contingency with the higher rank. The obtained results indicate that outages of branches 1-2, 28-27, and 27-30 are identified as the most severe contingencies among the other branch outage cases.

Table 6. Results of the branch outage contingency ranking for IEEE 30-Bus system.

Rank	Branch Outage	λ^{max}	CPU Time (s)	
			Proposed	CPFLOW
1	1-2	1.2575	0.57	2.26
2	28-27	1.5173	0.58	2.27
3	27-30	2.0271	0.55	2.24
4	2-5	2.2107	0.57	2.26
5	27-29	2.2289	0.54	2.24
6	9-10	2.3951	0.58	2.27
7	4-12	2.4150	0.57	2.26
8	29-30	2.5819	0.57	2.25
9	12-13	2.6331	0.57	2.26
10	6-8	2.6630	0.58	2.26
11	22-24	2.7053	0.56	2.27
12	12-15	2.7439	0.57	2.26
13	9-11	2.7808	0.57	2.25
14	15-23	2.7828	0.56	2.24
15	6-28	2.7883	0.56	2.24
16	6-9	2.7885	0.56	2.24
17	10-20	2.8045	0.57	2.25
18	2-6	2.8076	0.56	2.23
19	10-21	2.8089	0.57	2.26
20	8-28	2.8351	0.57	2.27
21	24-25	2.8471	0.55	2.23
22	2-4	2.8531	0.54	2.24
23	23-24	2.8735	0.56	2.23
24	6-10	2.8750	0.58	2.27
25	4-6	2.8781	0.56	2.23
26	1-3	2.8908	0.55	2.24
27	3-4	2.8989	0.56	2.26
28	12-16	2.9045	0.56	2.25
29	25-27	2.9046	0.54	2.23
30	19-20	2.9116	0.55	2.24
31	12-14	2.9149	0.54	2.23
32	10-22	2.9152	0.55	2.24
33	5-7	2.9207	0.55	2.24
34	15-18	2.9238	0.57	2.25
35	16-17	2.9311	0.55	2.25
36	18-19	2.9324	0.55	2.23
37	14-15	2.9329	0.57	2.26
38	21-22	2.9336	0.56	2.23
39	10-17	2.9357	0.57	2.26
40	6-7	2.9388	0.56	2.24
Total CPU Time (s)			**22.42**	**89.93**

The last two columns of Table 6 represent the execution times required for the proposed approach and conventional CPFLOW approach. It indicates that the proposed method can highly reduce the computation burden while maintaining λ^{max} accuracy.

Table 7 shows some selected simulation results of single contingency cases for the test systems. An inspection of this table clearly observes that the proposed method can work properly not only for line outage cases but also for generator outage cases.

Table 7. Selected Results of single contingency cases for test systems.

Test System	Out of Service	λ^{max}	VSM (%)
IEEE 30-bus	G8	1.1638	16.38
	G13	1.2144	21.44
	Line 1-2	1.2575	25.75
	Line 28-27	1.5173	51.73
IEEE 118-bus	G10	1.2387	23.87
	G24	1.3142	31.42
	Line 18-19	1.5216	52.16
	Line 63-64	1.4674	46.74
Taipower	G11	1.1136	11.36
	G42	1.1597	15.97
	Line 30-100	1.3742	37.42
	Line 220-223	1.2961	29.61

3.6. Comparison with Machine Learning Tools

The performance of the proposed method has been compared with two machine learning methods: the artificial neural network (ANN) method [15] and regression tree (RT) method [16]. Note that both the ANN method [15] and RT method [16] use VSM determined by CPFLOW as target output. In other words, both the ANN method [15] and RT method [16] can only give the results that are very close to or equal to those of CPFLOW.

Table 8 demonstrates the prediction of the VSM via the proposed method, ANN method [15], and RT method [16] under the selected cases listed in Table 1 for Taipower system. On comparing the predicted VSMs for the cases in Table 8, it is clearly seen that the proposed method was able to provide the best results, which were the same as the actual ones.

Table 8. Performance evaluation between the compared methods under the selected cases for Taipower system [1].

Case	VSM (%)			
	ANN [15]	RT [16]	Proposed	Actual
1	22.61	22.43	23.16	23.16
2	18.33	18.26	18.69	18.69
3	9.28	9.25	9.56	9.56

[1] ANN, artificial neural network; RT, regression tree.

3.7. Comparison with Line Voltage Stability Index

As mentioned previously, different voltage stability indices may give different results, especially for large-scale power grids [27]. A comparison study of the results obtained by the proposed method and voltage collapse proximity indicator (VCPI) method [26] for line outage contingency ranking is demonstrated here. Note that theoretically the value of VCPI ranges from 0 to 1, and it approaches 1 when the operating point is close to the voltage-collapse point [26].

In the simulation, all the loads including active and reactive powers in the test system are increased simultaneously based on their initial load levels. Table 9 illustrates the comparison results of the most critical lines under heavy load condition for Taipower system. In Table 9, one can see that different methods indeed give different ranking of critical lines. However, the results of the most critical lines obtained by the two compared methods are almost the same.

Table 9. Results of the most critical lines under heavy load condition for Taipower system [1].

Proposed			VCPI [26]		
Rank	**Line Outage**	**Value**	**Rank**	**Line Outage**	**Value**
1	2480-530	1.0775	1	2480-530	0.9439
2	1000-2950	1.0826	2	2950-2930	0.8864
3	2950-2930	1.1019	3	1000-2950	0.8736
4	2900-2950	1.1109	4	1080-2670	0.8548
5	1080-2670	1.1163	5	2900-2950	0.8312
6	2750-2660	1.1295	6	2750-2660	0.7861
7	2490-2500	1.1375	7	2490-2500	0.7345
8	2670-2650	1.1493	8	1080-2660	06767
9	2900-2750	1.1536	9	2670-2650	0.6553
10	2650-2600	1.1654	10	2900-2750	0.5651

[1] VCPI, voltage collapse proximity indicator.

4. Conclusions

A computationally efficient method for the determination of VSM in a large-scale power grid is proposed. This method combines both impedance match-based technique and model-based technique to quickly estimate the voltage collapse point. It also considers the generator Q limits for practical operation. Numerical examples for some standard IEEE test systems and Taipower system have been conducted. The simulation results are promising and confirm the effectiveness of the proposed method. Furthermore, a comparative study and analysis of the proposed method and VCPI method for line outage contingency ranking of Taipower system was carried out, showing that the results of the most critical lines obtained from both methods are almost the same.

Acknowledgments: This work was supported by the Ministry of Science and Technology of Taiwan, under contracts MOST 104-2221-E-035-041.

Conflicts of Interest: The author declares no conflict of interest.

References

1. Kundur, P. *Power System Stability and Control*; McGraw-Hill: New York, NY, USA, 1994.
2. Taylor, C.W. *Power System Voltage Stability*; McGraw-Hill: New York, NY, USA, 1994.
3. Su, H.Y.; Chen, Y.C.; Hsu, Y.L. A synchrophasor based optimal voltage control scheme with successive voltage stability margin improvement. *Appl. Sci.* **2016**, *6*, 1–12. [CrossRef]
4. Kundur, P.; Paserba, J.; Ajjarapu, V.; Andersson, G.; Bose, A.; Canizares, C.; Hatziargyriou, N.; Hill, D.; Stankovic, A.; Taylor, C.; et al. Definition and classification of power system stability IEEE/CIGRE joint task force on stability terms and definitions. *IEEE Trans. Power Syst.* **2004**, *19*, 1387–1401.
5. Morison, G.K.; Gao, B.; Kundur, P. Voltage stability analysis using static and dynamic approaches. *IEEE Trans. Power Syst.* **1993**, *8*, 1159–1171. [CrossRef]
6. Andersson, G.; Donalek, P.; Farmer, R.; Hatziargyriou, N.; Kamwa, I.; Kundur, P.; Martins, N.; Paserba, J.; Pourbeik, P.; Sanchez-Gasca, J.; et al. Causes of the 2003 major grid blackouts in north America and Europe, and recommended means to improve system dynamic performance. *IEEE Trans. Power Syst.* **2005**, *20*, 1922–1928. [CrossRef]
7. Ajjarapu, V. *Computational Techniques for Voltage Stability Assessment and Control*; Springer: New York, NY, USA, 2006.
8. Simpson-Porco, J.W.; Dörfler, F.; Bullo, F. Voltage collapse in complex power grids. *Nat. Commun.* **2016**. [CrossRef] [PubMed]
9. Begovic, M.; Fulton, D.; Gonzalez, M.R. Summary of system protection and voltage stability. *IEEE Trans. Power Del.* **1995**, *10*, 631–638. [CrossRef]
10. Schlueter, R.A. A voltage stability security assessment method. *IEEE Trans. Power Syst.* **1998**, *13*, 1423–1438. [CrossRef]

11. Flatabo, N.; Ognedal, R.; Carlsen, T. Voltage stability condition in a power transmission system calculated by sensitivity methods. *IEEE Trans. Power Syst.* **1990**, *5*, 1286–1293. [CrossRef]
12. Flatabo, N.; Fosso, O.; Ognedal, R.; Carlsen, T. A method for calculation of margins to voltage instability applied on the Norwegian system for maintaining required security level. *IEEE Trans. Power Syst.* **1993**, *8*, 920–928. [CrossRef]
13. Tiranuchit, A.; Thomas, R.J. A posturing strategy against voltage instabilities in electric power systems. *IEEE Trans. Power Syst.* **1988**, *3*, 87–93. [CrossRef]
14. Gao, B.; Morison, G.K.; Kundur, P. Voltage stability evaluation using modal analysis. *IEEE Trans. Power Syst.* **1992**, *7*, 1529–1542. [CrossRef]
15. Zhou, D.Q.; Annakkage, U.D.; Rajapakse, A.D. Online monitoring of voltage stability margin using an artificial neural network. *IEEE Trans. Power Syst.* **2010**, *25*, 1566–1574. [CrossRef]
16. Zheng, C.; Malbasa, V.; Kezunovic, M. Regression tree for stability margin prediction using synchrophasor measurements. *IEEE Trans. Power Syst.* **2013**, *28*, 1978–1987. [CrossRef]
17. Vu, K.; Begovic, M.M.; Novosel, D.; Saha, M.M. Use of local measurements to estimate voltage-stability margin. *IEEE Trans. Power Syst.* **1999**, *14*, 1029–1035. [CrossRef]
18. Smon, I.; Verbic, G.; Gubina, F. Local voltage-stability index using Tllegen's theorem. *IEEE Trans. Power Syst.* **2006**, *21*, 1267–1275. [CrossRef]
19. Corsi, S.; Taranto, G.N. A real-time voltage instability identification algorithm based on local phasor measurements. *IEEE Trans. Power Syst.* **2008**, *23*, 1271–1279. [CrossRef]
20. Su, H.Y.; Liu, C.W. Estimating the voltage stability margin using PMU measurements. *IEEE Trans. Power Syst.* **2016**, *31*, 3221–3229. [CrossRef]
21. Iba, K.; Suzuli, H.; Egawa, M.; Watanabe, T. Calculation of the critical loading with nose curve using homotopy continuation method. *IEEE Trans. Power Syst.* **1991**, *6*, 584–593. [CrossRef]
22. Ajjarapu, V.; Christy, C. The continuation power flow: A tool for steady state voltage stability analysis. *IEEE Trans. Power Syst.* **1992**, *7*, 416–423. [CrossRef]
23. Canizares, C.A.; Alvarado, F.L. Point of collapse and continuation methods for large AC/DC systems. *IEEE Trans. Power Syst.* **1993**, *8*, 1–8. [CrossRef]
24. Chiang, H.D.; Flueck, A.J.; Shah, K.S.; Balu, N. CPFLOW: A practical tool for tracing power system steady-state stationary behavior due to load and generation variations. *IEEE Trans. Power Syst.* **1995**, *10*, 623–634. [CrossRef]
25. Moghavvemi, M. New method for indicating voltage stability in power system. In Proceedings of the IEEE International Conference on Power Engineering, Singapore, 22–24 May 1997; pp. 223–227.
26. Moghavvemi, M.; Faruque, O. Real-time contingency evaluation and ranking technique. *IEE Proc.-Gener. Transm. Distrib.* **1998**, *5*, 517–524. [CrossRef]
27. Cupelli, M.; Doig Cardet, C.; Monti, A. Comparison of line voltage stability indices using dynamic real time simulation. In Proceedings of the 3rd IEEE PES International Conference and Exhibition on Innovative Smart Grid Technologies (ISGT Europe), Berlin, Germany, 14–17 October 2012; pp. 1–8.
28. Cupelli, M.; Doig Cardet, C.; Monti, A. Voltage stability indices comparison on the IEEE-39 bus system using RTDS. In Proceedings of the IEEE International Conference on Power System Technology (POWERCON), Auckland, New Zealand, 30 October–2 November 2012; pp. 1–6.
29. De Boor, C. *A Practical Guide to Splines*; Springer: New York, NY, USA, 1978.
30. Mathworks, Inc., Mathworks Matlab. Available online: http://www.mathworks.com/ (accessed on 4 March 2016).
31. Power Systems Test Case Archive, University of Washington College of Engineering. Available online: http://www.ee.washington.edu/re-serach/pstcal/ (accessed on 4 March2016).

© 2016 by the author; licensee MDPI, Basel, Switzerland. This article is an open access article distributed under the terms and conditions of the Creative Commons Attribution (CC-BY) license (http://creativecommons.org/licenses/by/4.0/).